Brain Material Properties and Integration of Arachnoid Complex for Biofidelic Impact Response for Human Head Finite Element Model

Aleksander Rycman[1], Michael Bustamante[1], Duane S. Cronin[1]

[1]Department of Mechanical & Mechatronics Engineering, University of Waterloo, 200 University Avenue West, Waterloo, Canada

Submitted to: Annals of Biomedical Engineering

Corresponding Author:
Dr. Duane S. Cronin
Department of Mechanical and Mechatronics Engineering
University of Waterloo
200 University Ave. West
Waterloo, Ontario, Canada, N2L 3G1
duane.cronin@uwaterloo.ca
(519) 888-4567 x32682

Abstract

Finite element head models offer great potential to study brain-related injuries; however, at present may be limited by geometric and material property simplifications required for continuum-level human body models. Specifically, the mechanical properties of the brain tissues are often represented with simplified linear viscoelastic models, or the material properties have been optimized to specific impact cases. In addition, anatomical structures such as the arachnoid complex have been omitted or implemented in a simple lumped manner.

Recent material test data for four brain regions at three strain rates in three modes of loading (tension, compression, and shear) was used to fit material parameters for a hyper-viscoelastic constitutive model. The material model was implemented in a contemporary detailed head finite element model. A detailed representation of the arachnoid trabeculae was implemented with mechanical properties based on experimental data. The enhanced head model was assessed by re-creating 11 ex-vivo head impact scenarios and comparing the simulation results with experimental data.

The hyper-viscoelastic model faithfully captured mechanical properties of the brain tissue in three modes of loading and multiple strain rates. The enhanced head model showed a high level of biofidelity in all re-created impacts in part due to the improved brain-skull interface associated with implementation of the arachnoid trabeculae.

The enhanced head model provides an improved predictive capability with material properties based on tissue level data and is positioned to investigate head injury and tissue damage in the future.

Keywords: brain tissue, traumatic brain injury, head model, finite element, quasi-linear viscoelasticity

Nomenclature

Abbreviations

CG	Center of Gravity
CORA	Cross Correlation Analysis
CSF	Cerebrospinal Fluid
FE	Finite Element
GHBMC	Global Human Body Model Consortium
HM_{50}	Head Model 50th Percentile Male
$HM_{50\text{-}E}$	Enhanced Head Model 50th Percentile Male
NDT	Neutral Density Target
TBI	Traumatic Brain Injury
QLV	Quasi-Linear Viscoelastic

Symbols

E	Young's modulus
$G(t)$	Viscoelastic function
G_i	Relaxation modulus
J	Relative volume
K	Bulk modulus
α_i, μ_i	Ogden model coefficients
β_i	Decay constants
ε	Strain
λ_i^*	Deviatoric principal stretch
ν	Poisson's ratio
ρ	Density
σ^E	Elastic stress

Introduction

Road traffic injury epidemiological data reports that 69 million people suffer traumatic brain injuries (TBIs) annually. Further, North America has the highest incidence rate of 1,299 TBI cases per 100,000 people.[8] According to the National Center for Injury Prevention and Control, in 2013, 2.8 million TBI-related injuries occurred in the United States alone.[50] TBI can result from various impacts, including sports injuries, motor vehicle accidents, falls and violence.[18] A postulated mechanism of TBI involves transfer of forces to brain tissue that cause deformation beyond the physiological range. Low stiffness and fragile cranial nervous tissues are enclosed in the skull, creating an isolated protective structure and complicating investigation of in-situ deformations.[33] Computational finite element (FE) models have been investigated as a method with great potential to study brain-related injuries.[45] Complex FE models require accurate geometrical representation, biofidelic material models, and application-specific hierarchical validation and verification.[6]

Physics-based brain FE models offer a promising opportunity for advancing TBI prediction beyond the scope of global head kinematics alone.[24] Using these models, researchers can investigate the probability of injury at the tissue level including the precise location and extent of structural damage. Several FE head models have been developed and applied to assess TBI risk with varying levels of success.[7,29,34,35,48,52] Accurate representation of the head and brain geometry can be achieved through medical imaging techniques (e.g., magnetic resonance imaging, computed tomography) with sub-millimeter precision. In contrast, measuring the mechanical response of the cranial nervous tissues presents many challenges. The mechanical response of the nervous system tissues has been reported to be nonlinear, asymmetric and viscoelastic.[26,30,31,47] Although a wide range of tissue mechanical data exists, often simple approaches are used to represent brain tissue in FE models. For example, linear-viscoelasticity has been frequently used to represent brain tissue in many current FE head models. [23,34,35,48,52] Although such constitutive models are widely available in commercial FE codes and are computationally stable, they have recognized limitations in accurately representing the nonlinearity and asymmetry reported from experimental tests on brain tissue.[34] In some cases, the material parameters of a model have been optimized to the target experimental data to improve model results.[24] Miller et al.[35] acknowledged a large range of reported linear viscoelastic parameters for brain tissue, some of them (e.g., G_0) varying by as much as two orders of magnitude, and proposed linear viscoelastic material parameters optimized to experimental impact scenarios using FE models. Developers of FE models have also utilized hyper-viscoelastic material models to represent brain tissue.[15,16,32,44,49,51,54] An optimization approach was undertaken by Lyu et al.[32] and Zhou et al.[55] where material model parameters were optimized by comparing the mechanical response of the brain tissue in a FE model to brain deformation measured in cadaver head impact tests using high-speed x-ray imaging of implanted neutral density targets (NDTs).[20,21] Giudice et al.[16] calibrated an infinitesimal shear modulus to measured 3D brain deformation during in-vivo mild head impacts, and assessed material model non-linearity using high severity rotational head kinematic loading conditions.[1]

Experimental investigation of the deformation of human brain tissue under impact loading conditions revealed relatively more deformation at the center of the brain compared to the deformation observed closer to the surface of the brain.[20] Jin et al.[25] inferred that the arachnoid trabeculae was essential in

anchoring the brain within the skull, limiting the relative motion between the brain and the skull. Additionally one FE study, investigated detailed model of the arachnoid trabeculae implemented in the immature piglet FE model and concluded that inclusion of those structures improved predictions of haemorrhage at the brain-skull interface.[46] Cerebrospinal fluid (CSF) and trabeculae are critical in the motion of the brain since they surround the brain and transfer external impact forces from the skull to the brain. At present, trabeculae have not been implemented in detailed FE head models used for human safety. Instead, in some FE models, the effect of the trabeculae was approximated by assigning a shear stiffness to the CSF.[28,32,34] Moreover, for numerical stability reasons, CSF was modelled with a reduced bulk modulus, thus having lower bulk stiffness than the intended material.[32]

Multiple experimental studies have reported mechanical testing on brain tissue.[22,39,40,47] Animal specimens, mostly porcine and bovine, were utilized due to the availability of material and shortest post-mortem time.[5,22,30,31,39,47] Some studies have tested brain tissue from post-mortem human subjects.[9,10,26] Most of the studies focused on response of the brain tissue in a single mode of loading; most commonly, compressive properties were reported. Three journal papers reported multi-modal i.e., compressive, tensile, and shear properties of brain tissue from two experimental data sets.[26,30,31] Li et al.[30,31] performed mechanical testing of porcine brain tissue within 6 to 8 hours after post-mortem. Whereas Jin et al.[25] performed mechanical testing within an average post-mortem time of 4 days, before testing the specimens were kept at 4 °C. Regarding dynamic properties of the brain tissue, most studies focused on quasi-static to intermediate rates (< 100 s^{-1}). The stress-strain curves at a very wide range of strain rate, from 0.01 s^{-1} to 3000 s^{-1}, were reported in one study; however, only in compression.[38,39] Mechanical properties of brain tissue under multiple strain rates ranging from quasi-static up to 50 s^{-1} were reported by two studies.[26,30,31]

The objective of the present study was to enhance a contemporary detail head finite element model by (1) calibrating material models for the brain tissue that were based on measured mechanical properties of brain tissue; (2) defining an anatomically accurate representation of the skull-brain interface by implementing arachnoid trabeculae, and (3) validating the enhanced model using independent experimental data. As a first step, recently published dynamic multi-modal brain tissue experimental data was fitted to a hyper-viscoelastic material model, and a discrete arachnoid representation was integrated into the FE head model. Validation of the brain tissue response and intracranial pressure during dynamic impact and rotation of the head was performed by re-creating 11 ex-vivo experiments, and comparing a total of 74 brain tissue time-deformation curves and 3 time-pressure curves.[1,20,21,36] Lastly, comparison between the baseline model and the enhanced model was conducted.

Methods

Enhancement of a Detailed Finite Element Head Model

The current version of the GHBMC average stature male head model (version 6.0), representing a 50th percentile male, was used as a baseline model for the current study.[32] The baseline model was labelled HM_{50}. The geometry of the HM_{50} was based on subject-specific magnetic resonance imaging scans, collected using a 1.5T Twin Speed scanner (GE, Milwaukee, WI) with a matrix resolution of 589x192

pixels.[13] The model was grouped into parts corresponding to the anatomical structures, i.e., bones, skin, flesh, meninges, CSF, and cranial central nervous tissues: cerebellum, cerebrum, corpus callosum, thalamus, brainstem. The brain tissue was meshed using selectively reduced integrated elements (LS-DYNA solid element formulation -1) that eliminated the need for hourglass energy control while not being susceptible to shear locking.[17] Additionally, changing to this new element formulation did not require modifications to the brain tissue mesh. The mesh quality of the HM_{50} was reported previously[32,34] and does include some quality elements that should be investigated in future studies. The HM_{50} head model was enhanced in 2 areas: the mechanical properties of the brain tissue, and implementation of the arachnoid trabeculae. The enhanced model was denoted as $HM_{50\text{-}E}$ in this study (Figure 1).

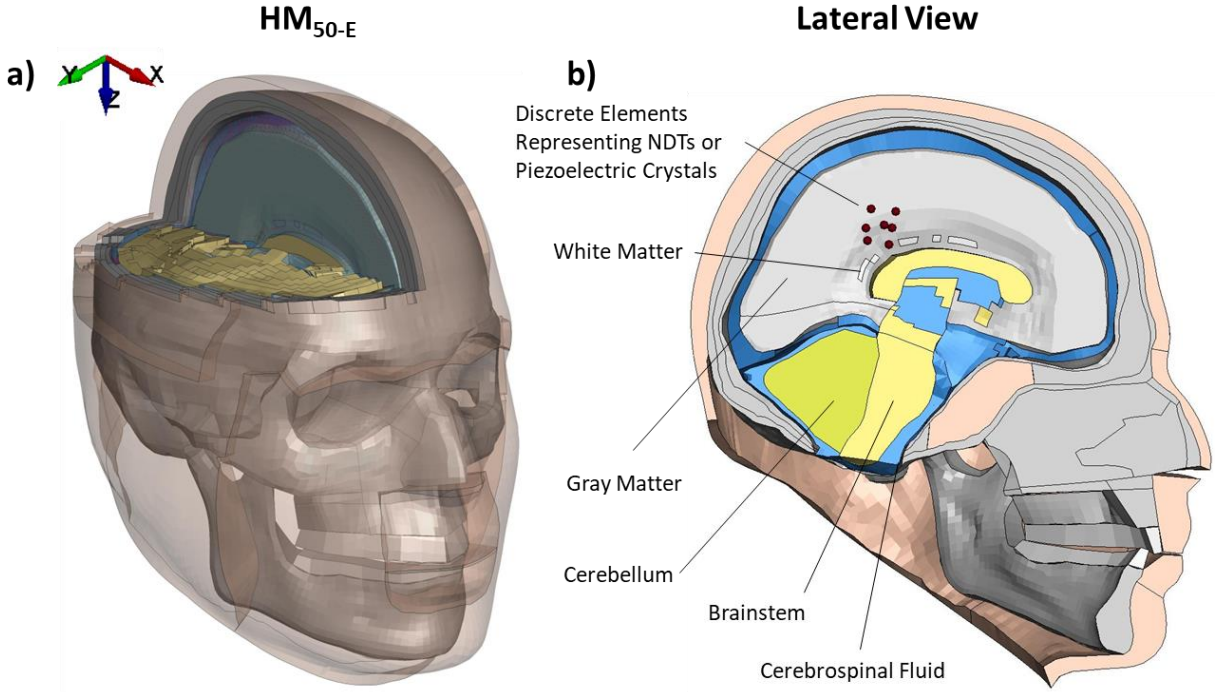


Figure 1: Cut-away views of the $HM_{50\text{-}E}$ head model: a) sectional view of the head model, b) lateral view of the head model with parts labelled and showing experimental location of neutral density targets or crystals for measuring brain deformation.

Material Properties of the Brain Tissue and CSF Constitutive Models

Brain tissue is a compliant, rate dependent, and nonlinear biological material with distinct asymmetry between tension and compression.[26] Previously reported experimental data[30,31] that characterized mechanical response of the brain tissue was used to fit the material parameters of a hyper-viscoelastic model based on an Ogden hyperelastic function. This modeling approach is often termed quasi-linear viscoelasticity (QLV), and is referred to as hyper-viscoelastic in this study. Li et al.[30,31] reported data from four porcine brain regions: white matter, gray matter, brainstem, and cerebellum. Specimens from each region were tested under three strain rates (0.01 s^{-1}, 1 s^{-1}, and 50 s^{-1}) and three modes of loading: tension, compression, and shear. In total, thirty-six stress-strain curves, nine for each region, were

digitized (CurveExpert, Hyams Development) and used to fit four sets of parameters for the hyper-viscoelastic model, one set for each brain region that was tested. Experimental data from Li et al.[30,31] was used in the current study as the specimens were tested shortly after post-mortem (6 to 8 hours), over a wide strain rate range and in three modes of loading. The hyper-viscoelastic formulation utilized an Ogden strain energy density function with a normalized quasi-linear viscoelasticity implementation.[11,37]

$$W(\lambda_1,\lambda_2,\lambda_3) = \sum_{i=1}^{N} \frac{\mu_i}{\alpha_i}\left(\lambda_1^{*\alpha_i} + \lambda_2^{*\alpha_i} + \lambda_3^{*\alpha_i} - 3\right) + \frac{1}{2}K(J-1)^2$$

Equation 1: The Ogden strain energy density function, including a hydrostatic component for implementation in a FE code.

$$\sigma(t) = \int_0^t \sum_{i=1}^{n} G_i e^{-\beta_i(t-\tau)} \left[\frac{\partial \sigma^E}{\partial \varepsilon}\frac{\partial \varepsilon}{\partial \tau}\right] d\tau$$

Equation 2: Total stress in the quasi-linear viscoelastic model as a function of time and deformation.

Four experimental data sets were considered, corresponding to measured stress-strain curves for four brain regions: white matter, gray matter, brainstem, and cerebellum. The fitting method followed a previously proposed method to optimize hyper-viscoelastic material coefficients for the spinal cord tissue under compressive loading.[41] Some modifications were required for the current study, with 9 stress-strain curves for each of the four brain regions: three modes of loading and three deformation rates. For each experimental data set, corresponding to one brain region, a two-term (N=2) quasi-static hyperelastic function was fitted to the tensile and compressive portion of the stress-strain curve at the lowest rate (i.e., 0.01 s^{-1}). The shear response was not directly fit, since the Ogden model determines this response from the tension and compression response. The viscoelastic portion of the experimental tension, compression and shear curves were simultaneously fit with two pairs of viscoelastic coefficients (G_i, β_i for n=2). The coefficients were optimized using a commercial optimization software (LS-OPT v6.0.0, ANSYS, Canonsburg) integrated with a commercial explicit FE solver (LS-DYNA R10.1 double-precision, ANSYS, Canonsburg). The optimization algorithm minimized the difference in area under the curves, for the experimental and simulated stress-strain curves. The optimization process was repeated for each brain region, therefore four sets of the hyperelastic and viscoelastic coefficients were determined along with the coefficients of determination (R^2). For the sake of comparative analysis, the material model used to represent gray matter in HM_{M50} was presented with the results of the fitting procedure.

CSF is mainly composed of water (99%) with a small concentration of proteins, ions, neurotransmitters, and glucose.[27] Therefore, the mechanical properties of CSF can be assumed to be similar to that of water.[4] A Newtonian fluid material model was previously used to represent mechanical properties of the

CSF in FE studies.[42,43] The Newtonian fluid model relates volumetric strains with constant bulk modulus to calculate the hydrostatic component of stress. The deviatoric part of stress is computed based on the deviatoric strain rate; however, since the viscosity of the CSF is small, the deviatoric portion of stress in the fluid was neglected.

Implementation of the Arachnoid Trabeculae

The arachnoid trabeculae are delicate fiber-like tissues that, with two other cranial meninges (pia and dura), protects and separates the cranial nervous tissues from the skull.[25] The arachnoid trabeculae was represented in the $HM_{50\text{-}E}$ by implementing one-dimension beam elements with tension-only response between the pia mater and the arachnoid mater (Figure 1a). The tension modulus (12.6 kPa) was based on average experimental measurements of human pia-arachnoid complexes tested in normal traction loading (Table 1).[3] Each beam element connects one node from the arachnoid mater to one node from the pia mater (Figure 2). The outer elements of the pia mater vary in area; therefore, it was necessary to compute each beam circular cross-sectional area separately to achieve the target modulus of 12.6 kPa via the beam element stiffness. The trabeculae beam cross-sectional area was calculated based on the average surface area of the pia mater elements that are connected to it (Figure 2).

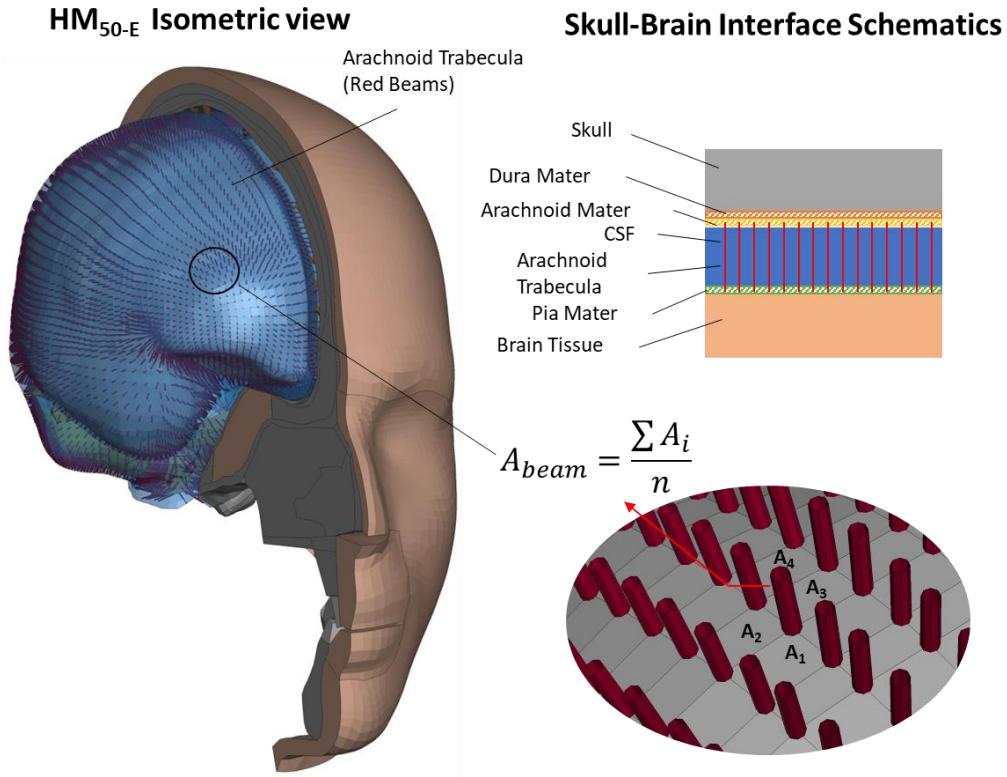


Figure 2: Isometric view of the head (left) showing the distribution of arachnoid trabecula (red elements) with a zoomed surface of the brain (bottom right) and a labeled schematic of the skull-brain interface (top right).

Table 1: Mechanical properties of the cranial nervous system tissues used in the $HM_{50\text{-}E}$.

Material	Constitutive Law	Material Properties			Reference
Brainstem	Hyper-viscoelastic	μ_1 = 1.621 [MPa]	$\alpha_1 = 1.12*10^{-3}$	ν = 0.49999	Li et al.[30,31]
		μ_2 = -7.822 [Pa]	α_2 = -5.41	ρ = 1060 kgm^{-3}	
		G_1 = 0.319	$\beta_1 = 1\ s^{-1}$		
		G_2 = 0.429	$\beta_2 = 50\ s^{-1}$		
Cerebellum	Hyper-viscoelastic	μ_1 = 1.600 [MPa]	$\alpha_1 = 1.1*10^{-3}$	ν = 0.49999	
		μ_2 = -0.716 [Pa]	α_2 = -5.12	ρ = 1060 kgm^{-3}	
		G_1 = 0.259	$\beta_1 = 1\ s^{-1}$		
		G_2 = 0.382	$\beta_2 = 50\ s^{-1}$		
Gray matter	Hyper-viscoelastic	μ_1 = 1.468 [MPa]	$\alpha_1 = 1.01*10^{-3}$	ν = 0.49999	
		μ_2 = -6.424 [Pa]	α_2 = -5.07	ρ = 1060 kgm^{-3}	
		G_1 = 0.231	$\beta_1 = 1\ s^{-1}$		
		G_2 = 0.384	$\beta_2 = 50\ s^{-1}$		
White matter	Hyper-viscoelastic	μ_1 = 1.687 [MPa]	$\alpha_1 = 1.16*10^{-3}$	ν = 0.49999	
		μ_2 = -0.555 [Pa]	α_2 = -8.30	ρ = 1060 kgm^{-3}	
		G_1 = 0.213	$\beta_1 = 1\ s^{-1}$		
		G_2 = 0.483	$\beta_2 = 50\ s^{-1}$		
CSF	Newtonian fluid	K = 2.19 GPa		ρ = 1060 kgm^{-3}	
Arachnoid Trabecula	Elastic cable	E = 12.6 kPa		ρ = 1030 kgm^{-3}	Benko et al.[3]

Validation Test Cases for the* $HM_{50\text{-}E}$ *Enhanced FE Head Model

To validate the $HM_{50\text{-}E}$, experimental loading conditions were re-created and integrated with the enhanced head model. The models were solved in a commercial FE code (LS-DYNA R12 single-precision, ANSYS, Canonsburg), and the simulation results were compared to the reported data. The re-created experiments included measurements of the brain tissue motion during impacts on cadaveric heads, and high-speed rotational motions applied to cadaveric heads.[1,15,16] Further, the head model was validated using CSF pressure resulting from experimental impacts to PMHS heads.[36] The baseline head model (HM_{50}) was also simulated in the validation cases and results were compared.

Hardy et al.[20,21] conducted a series of impacts on cadaveric heads with radio-opaque neutral density targets (NDTs) embedded in the brain tissue. Each impact test was recorded with a system of high-speed X-ray cameras that allowed the acquisition of the displacements of the NDTs and the head CG. The initial position and displacements of each NDT were reported, with respect to the cadaver head CG. The experimental head CG acceleration-time curves were used as an input to the $HM_{50\text{-}E}$ for six reported experimental impacts (tests C288-T3, C380-T3, C380-T4, C383-T3, C383-T4, and C755-T2). The NDTs were implemented as discrete elements in the model using reported masses and moments of inertia

(Figure 1b). A total of 38 experimental NDTs displacements were compared using cross-correlation analysis (CORA) with the simulation results.[14] The NDT naming convention in the current study was taken from the original experimental work, and each NDT trace was labeled as follows 'Test Identification NDT-Number Direction' e.g., C288-T3 NDT-4 X.[19]

Alshareef et al.[1] undertook a series of experiments to measure brain motion during rotational motion of the head in the coronal plane. Triangulation and sonomicrometry was used to determine the relative displacement of piezoelectric crystals with respect to the skull.[2] The piezoelectric crystals were implemented in the cadaver brain and the receiver sensors were glued to the cadaver skull. The experimental rotational signals of the head CG in the coronal plane were digitized and prescribed to the $HM_{50\text{-}E}$ (Figure 2). Prescribed rotational velocity signals were approximately sinusoidal, with two different pulse magnitude (20 and 40 radians per second) and duration (30 and 60 ms), creating four different combinations: 20rps_30ms, 20rps_60ms, 40rps_30ms and 40rps_60ms. The discrete elements representing the 9th, 16th and 31st experimental piezoelectric crystals (receivers) were implemented in the $HM_{50\text{-}E.}$ The time-displacement traces of the implemented discrete elements in the $HM_{50\text{-}E}$ with respect to the skull were compared with the published experimental piezoelectric crystal time-displacement traces. The naming convention for time-displacement traces was adopted as follows 'Crystal Number -Test-Direction' e.g., 16-20rps_60ms X.

Nahum et al.[36] performed a series of impacts on cadaveric heads with implemented pressure transducers in the subarachnoid space. The $HM_{50\text{-}E}$ was positioned as reported in the experimental protocol. The Frankfort anatomical plane was inclined 45 degrees to the horizontal plane. Experimental impacts were re-created by applying the measured force-time signal to the $HM_{50\text{-}E}$ skull. The cerebrospinal fluid pressure was monitored, and results from three locations: frontal, parietal, and occipital, were compared to the experimental results. The simulation results were processed using a custom-written Python script and commercial post-processing software (LS-PrePost version 4.7.9).

All validation simulations terminated normally using single precision (LS-DYNA MPP R12) on 16 Intel Xeon E5-2683 2.1 GHz processors with an average wall-clock time of 114 ms/hour for HM_{50} and 27 ms/hour for $HM_{50\text{-}E}$. CORA (v3.0.0) cross-correlation analysis was performed on the displacement history results between the experiments and simulations. Only the cross-correlation rating scheme (G_2 = 1.0 and G_1 = 0.0) with the progression weighting (G_V = 0.5) and size weighting (G_G = 0.5) were used in the CORA analysis. The intention of only using the cross-correlation rating scheme was due to the lack of corridor data for each of the experimental NDTs, where automatic calculation of corridors may bias comparison of the results. Within the cross-correlation scheme, only the progression and size rating schemes were performed since the simulation cases were synchronized with the experimental data; therefore, shifting in time was unnecessary. The penalty exponent factor for progression (K_V = 1.0) was made linear. Lastly, the global parameters that were altered were the start (A_THRES = 0), end (B_THRES = 1), extension (A_EVAL = 0), and shortening parameter (B_DELTA_END = 0) of the interval of evaluation. These global parameters were set to ensure that the entirety of the signals was within interval of evaluation. All other parameters remained as their default for version v3.0.0 of CORA. Although the exclusion of the corridor rating scheme has been reported to increase the overall ratings[1], both models in the present study were assessed in the same manner using the same CORA parameters.

Results

The brain tissue material model optimization resulted in an overall good fit of the hyper-viscoelastic models to the dynamic multi-modal experimental data (Figure 3a). An average coefficient of determination (R^2) (Table 2) ranged from 0.41 for the region of the brain stem to 0.69 for the region of gray matter. All obtained models accurately represented the quasi-static compression and tension portions of the experimental curves (R^2 0.96 to 1.00). In general, the hyper-viscoelastic model fits underpredicted the quasi-static portion of the shear response and overpredicted the dynamic portion of tension responses (Figure 3, Table 2).

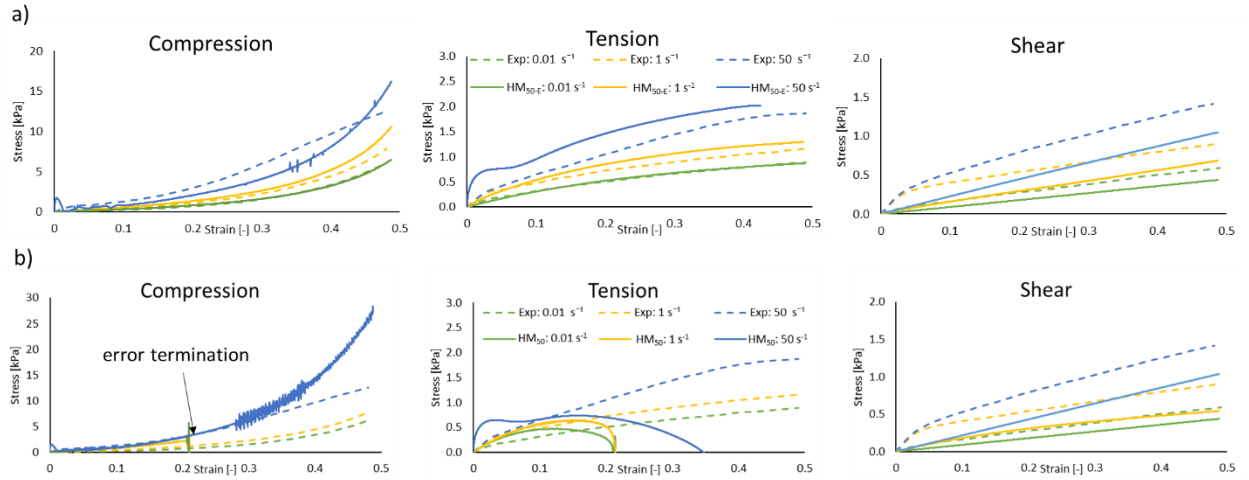
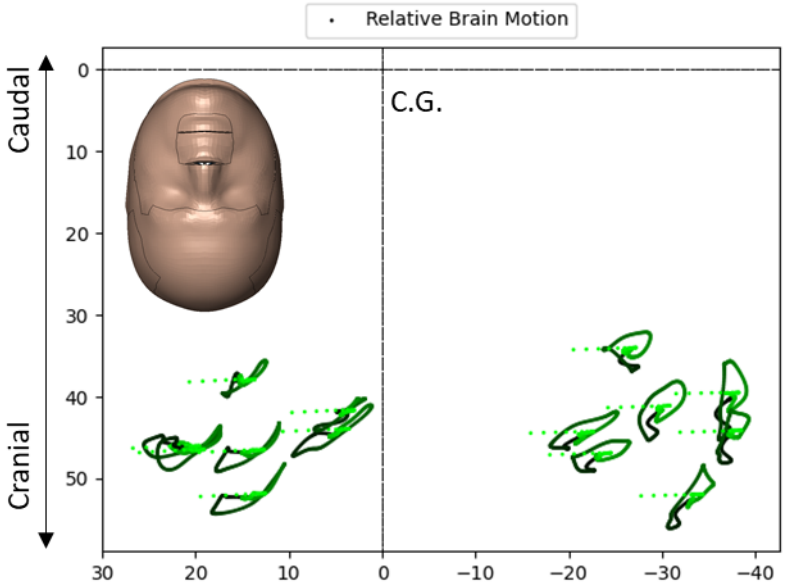


Figure 3: a) Fit of the optimized hyper-viscoelastic material model to the multi-modal experimental data; graphs showing fit to gray matter data in compression, tension, and shear for $HM_{50\text{-}E}$ (all graphs included in Appendix A1-A3) b) the material model used in the baseline GHBMC version (HM_{50}) to represent gray matter.

Table 2: Coefficient of determination (R^2) for individual strain-stress curve fits for brain tissue material used in the $HM_{50\text{-}E}$.

	Compression			Tension			Shear			Average
	0.01 s^{-1}	**1 s^{-1}**	**50 s^{-1}**	**0.01 s^{-1}**	**1 s^{-1}**	**50 s^{-1}**	**0.01 s^{-1}**	**1 s^{-1}**	**50 s^{-1}**	
White Matter	0.99	0.94	0.83	0.96	0.43	-0.33	0.45	0.26	0.67	0.58
Gray Matter	0.99	0.92	0.89	1.00	0.83	0.64	0.60	0.09	0.30	0.69
Cerebellum	0.99	0.99	0.65	0.98	-0.25	0.26	0.80	0.77	0.28	0.61
Brain Stem	0.99	0.97	0.86	0.99	-1.20	0.31	-0.90	0.85	0.78	0.41

Comparison of the simulation displacements from the re-created impact tests with reported experimental traces resulted in similar trends as reported in the experimental data (Figures 4 and 5).[20,21] All compared curves for the experiments are shown in the Appendix (Figure A4 to A8).



	Cora Score			
Signal	NDT-4 Y	NDT-4 Z	NDT-11 Y	NDT-11 Z
HM_{50}	0.842	0.534	0.729	0.690
$HM_{50\text{-}E}$	0.769	0.616	0.815	0.539

Figure 4: Head model predicted NDT displacement traces relative to the skull (test 380-T4).[21] Traces transition from green (start of simulation) to black (end of simulation).

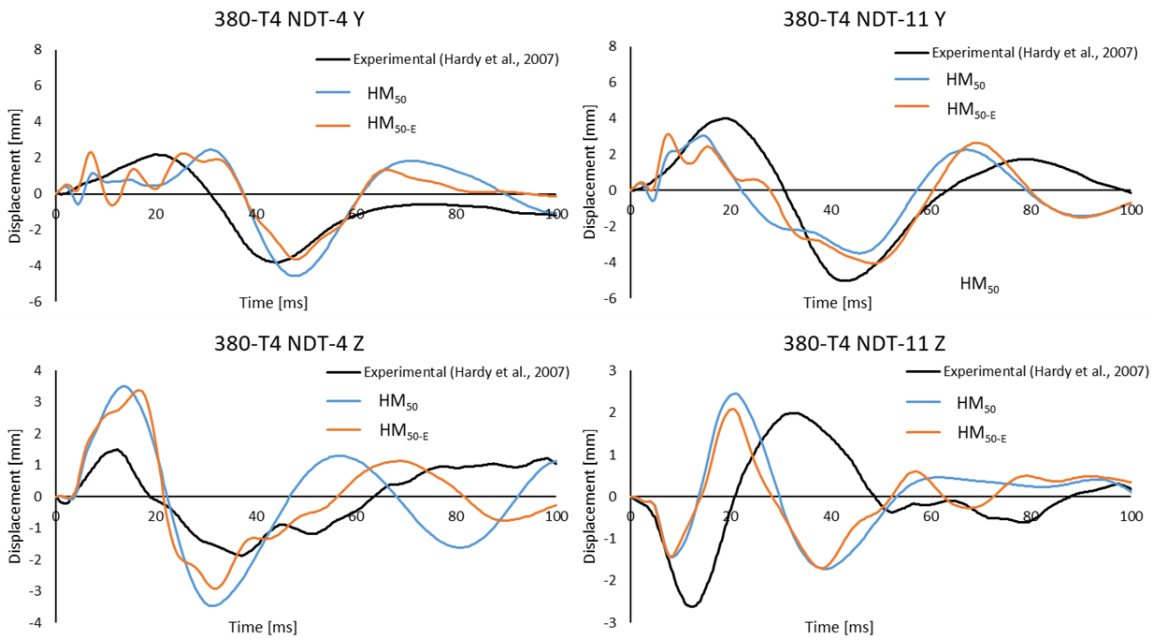


Figure 5: Exemplar time-displacement traces relative to the skull of the 4th and 11th NDTs compared to the experimental data from the impact test 380-T4 for the HM_{50} (blue line) and $HM_{50\text{-}E}$ (orange line).[21]

The $HM_{50\text{-}E}$ predicted with reasonable accuracy (±1 mm) the magnitude of the peaks of the NDT-4 Y, NDT-11 Y, and NDT-11 Z experimental traces in the 380-T4 experiment. However, for the NDT-4 Z time-displacement, the peak was overpredicted by 2.5 mm. The model correctly predicted or overpredicted the magnitude of deformation for time-displacement traces in all impacts simulated (Appendix, Figure A4-A8). The model showed fair to good cross-correlation ratings (0.501 to 0.686), with an average of 0.595 for all simulated impact cases. Similar results were obtained using the HM_{50} model (Table 3).

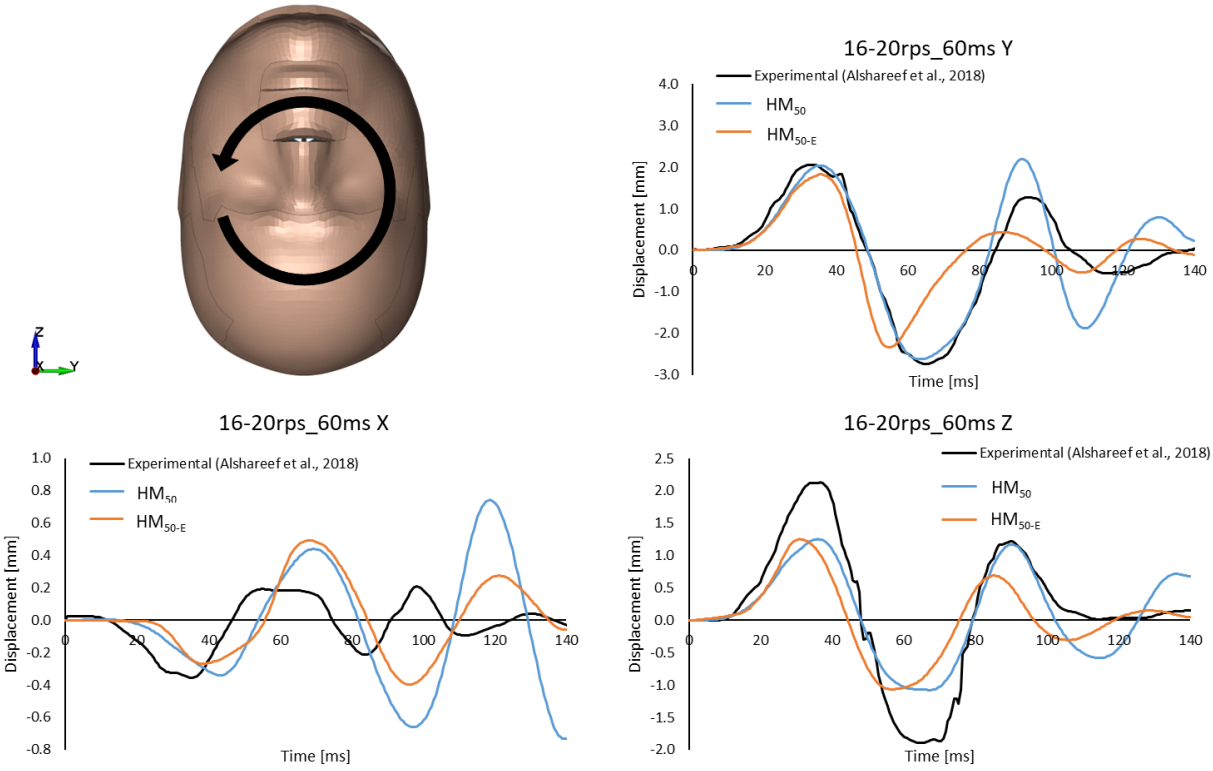


Figure 6: Exemplar results of the rotation simulation (20 radians per second) for the HM_{50} (blue line) and $HM_{50\text{-}E}$ (orange) compared to the experimental data for the 16th receiver in x, y and z directions.[1]

Comparison of the simulation results from re-created rotational brain motion tests showed a high correlation with experimental data (Appendix, Figure A9-A12).[1] Primary motion directions of the piezoelectric crystals (y and z) showed excellent correlation between the model and experimental data (Figure 6). The model overpredicted the x-displacement of all compared traces. Cross-correlation ratings ranged from 0.626 to 0.753, with an average rating of 0.704 (Table 3). In the 20rps_30ms test, a constant offset of approximately 20 ms in all compared curves was observed (Appendix, Figure A10). The GHBMC baseline model (HM_{50}) predicted similar traces, however the traces were more oscillatory between 80 and 120 ms.

Table 3: Summary of CORA ratings obtained from the re-creation of the head impacts and rotational experimental tests for HM_{M50} and $HM_{M50\text{-}E}$.

CORA Ratings							
Impact tests [20,21]							
	C288-T3	C380-T3	C380-T4	C383-T3	C383-T4	C755-T2	Average
HM_{M50}	0.589	0.710	0.699	0.608	0.526	0.578	0.618
$HM_{M50\text{-}E}$	0.501	0.686	0.685	0.588	0.514	0.598	0.595
Rotational tests[1]							
	20rps_60ms	20rps_30ms	40rps_60ms	40rps_30ms	Average		

HM_{M50}	0.636	0.654	0.681	0.535	0.627
$HM_{M50\text{-}E}$	0.704	0.730	0.753	0.626	0.704

The re-creation of experimental impacts conducted by Nahum et al.[36] resulted in slightly underpredicted pressure peaks in all three locations, 12.0% (15.3 kPa) in the frontal, 9.1% (-3.96 kPa) in the parietal, and 12.9% (8.52 kPa) in the occipital location (Figure 7).

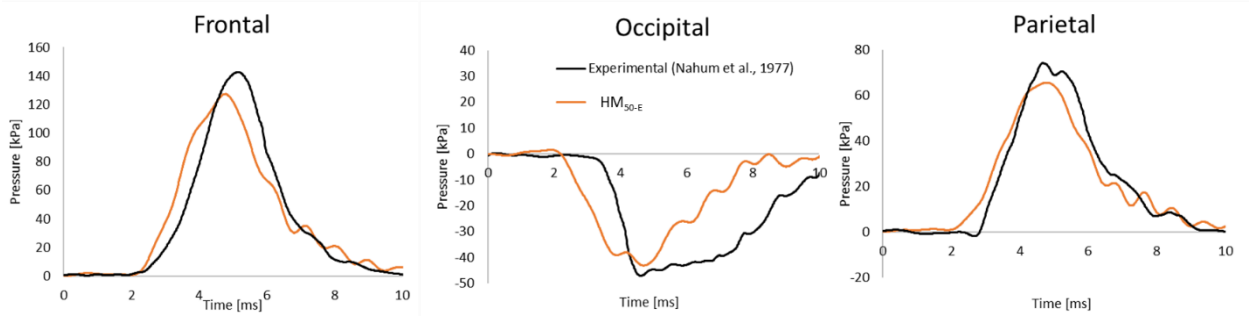


Figure 7: Comparison of the experimental (black) and simulated (orange) time-intracranial pressure signals obtained from three locations for the $HM_{50\text{-}E}$.

Discussion

The current study aimed to incrementally improve a head model (GHBMC) widely used by the academic community and automotive industry. Firstly, a novel contribution of the current study was to fit hyper-viscoelastic material model parameters to multi-modal dynamic tissue-level experimental data for four brain regions. Other approaches, such as that used for HM_{50}, developed brain tissue material models though optimization of NDT displacement and calculated strains.[32] Although such an optimization approach can calibrate the model to the targeted outcome, it is possible the material can exhibit unphysical response, as demonstrated for the tension mode of loading. While an optimized model may perform well for the specific optimized impact cases, it is possible that the results may not be biofidelic in other impact cases. Secondly, implementation of the arachnoid trabeculae accompanied with solid representation of CSF with fluid material model provided a more anatomically correct representation of the skull-brain interface, based on recent studies and literature data. However, modelling the skull-brain interface remains a challenge and further research is required.[24]

The mechanical data for brain tissue was fit to a two-term Ogden function and was able to represent the non-linearity and asymmetry between tension and compression for the quasi-static data. Tissue-level experimental data[30,31] was based on testing pediatric porcine specimens and was similar in response to tissue-level experimental data from human specimens.[26] Li et al.[30,31] tested over a broader range of strain rates and 6 to 8 hours after post-mortem; therefore, this data set was used to fit the material models. One limitation of the experimental data was that the shear data at 0.01 s^{-1} and 1.0 s^{-1} was similar. Therefore, the shear data was not used in the quasi-static fit. The data used in the current study represents an excellent data set to represent brain tissue under three primary modes of loading for four brain regions.[30,31]

The viscoelastic material properties were fit for all available stress-strain curves and demonstrated a good correlation, with averaged R^2 in the range between 0.41 and 0.69. In some cases, the R^2 parameter became negative (e.g., brain stem material model, tension, 1 s^{-1}), meaning that an average value provided better predictive capability compared to the hyper-viscoelastic model predictions. This is attributed to some challenges in the experimental data as noted above, but overall provided a good fit to the data. The fitted hyper-viscoelastic model was implemented into the FE head model and was stable for all impact cases considered in this study. In the current study we included material data for four brain regions as reported in Li et al.[30,31]

In addition, the brain-skull interface was improved by incorporating a CSF model with an experimentally measured bulk modulus, and implementation of arachnoid trabeculae. The arachnoid trabeculae mechanical properties were assigned reported values based on human tissue[3] that were more compliant (12.6 kPa) compared to previously reported (30.92 kPa) properties from bovine tissue.[25] The new implementation of the arachnoid trabeculae transfers tensile and shear loads between the skull-brain interface. Additionally, the implementation of the arachnoid trabeculae enables further research to explore model capabilities in predicting haemorrhage at the brain-skull interface.[46]

Validation of the $HM_{50\text{-}E}$ to the head impact data showed good CORA ratings for the simulated experiments in terms of signal magnitude and shape.[20,21 32] However, some oscillations were observed in the $HM_{50\text{-}E}$ response. The oscillations were attributed to the high bulk-to-shear modulus ratio within the model for the brain tissue, associated with the higher, but physically correct bulk modulus. Lyu et al.[32] calibrated an anisotropic hyper-viscoelastic material model and properties of the brain tissue to the impact test data.[20,21,55] However, the calibration proposed by Lyu et al. resulted in unphysical material parameters (opposite signs of the hyperelastic Mooney Rivlin coefficients).[32] The tissue level tension test showed that the calibrated material did not satisfy the Drucker stability postulate (Figure 3). Similar CORA ratings were obtained by HM_{50} and $HM_{50\text{-}E}$ in the impact simulations (Table 3). The calibrated linear viscoelastic brain material properties proposed by Miller et al.[35], that were optimized for the impact test data presented in Hardy et al.[20,21] resulted in a slightly lower CORA rating (0.424 to 0.491). It is worth noting that the FE Head model used by Miller et al.[35] used a simplified approach to represent the brain-skull interface where the relative motion of the CSF and skull was restricted. In the present study, the experimentally reported NDT displacements were compared directly to the predicted displacements from the corresponding markers in the model. Some researchers have calculated strain from the markers for comparison to FE model output, and this should be considered in future studies.[54,55]

Comparing the enhanced head model and experiments for the rotational experimental data in the primary directions of loading (i.e., y- and z- directions), resulted in an average CORA rating of 0.833. The x-direction was perpendicular to the coronal plane therefore the experimentally measured displacements were small, on the order of 1 mm. The $HM_{50\text{-}E}$ model predicted greater displacements in the x-direction compared to the experiments, which could be an outcome of different mesh size or numerical noise in the model, owing to the small displacements. Relatively small variations in predicted deformations could lead to large variations in CORA ratings since the displacements published in the experimental data were sub-millimeter, which has been observed in other numerical studies.[54] The

previous HM_{50} yielded similar CORA ratings for the primary loading directions (average of 0.76). However, the traces were more oscillatory (Figure 4; blue curves). A use of unphysical brain tissue coefficients in HM_{50} might be a cause of the oscillations. The observed time offset in the 20rps_30ms experimental test (~20 ms) stands out from the other experimental rotational cases. The model did not demonstrate this offset and further investigation is needed.

The current study has some recognized limitations. The maximum strain rate in the tissue level material tests was 50 s^{-1}, although higher deformation rates were predicted in the model. A benefit of the obtained hyper-viscoelastic models is the ability to extrapolate beyond the maximum experimental deformation rate of 50 s^{-1}; however, the viscoelastic extrapolation is linear, and additional experimental data is needed at higher deformation rates. In addition, viscoelastic terms corresponding to higher deformation rates can be added to the material models as new data becomes available. The material data was fit across the entire range of experimental data, for example up to 50% strain in tension. Other studies have reported functional damage to the nervous tissue at lower strain levels[12], and potentially structural damage in the brain tissue may occur at lower levels, which is not accounted for in a hyper-viscoelastic model. It is important for a constitutive model to predict response at high levels of strain, and high strain rates, and to be computationally stable throughout these large deformations and deformation rates. Future research should investigate the importance of regional brain property variation. A critical requirement for improved constitutive models is the need to incorporate material damage, and this will be critical for future applications in predicting tissue injury. Further refinement of the $HM_{M50\text{-}E}$ should include improvements of the mesh resolution and quality.[53,54] Future efforts should involve a validation of the HM_{M50} for low severity impacts and a single study should undertake direct comparison of various available head models. The proposed representation of the trabeculae was discreate elements, while the actual trabeculae exhibit a web-like structure. Further discretization can improve this representation. Finally, the trabeculae were modelled with a homogenous stiffness of 12.6 kPa based on experimental data.[3] Benko et al.[3] provided data on regional variation in the stiffness of the arachnoid trabeculae, and such variations should be considered in future versions of the model.

Conclusions

The brain material properties fitted to a hyper-viscoelastic model in this study were based on multi-modal tissue-level experimental data, providing a stable computational platform for assessing brain deformation over a range of impact scenarios. Validation of the enhanced head model in multiple impact scenarios showed that the proposed hyper-viscoelastic model and incorporation of arachnoid trabeculae provided good correlation with a wide variety of head impact scenarios. The introduction of trabeculae, in the form of discrete beam elements, represented the brain-skull interface and provided an anatomically improved representation of these important tissues. The enhanced head model provides a biofidelic predictive capability with foundational material properties and is positioned to investigate head injury and tissue damage in the future.

Conflict of Interest

The authors declare that the research was conducted in the absence of any commercial or financial conflict of interest.

Acknowledgement

The authors gratefully acknowledge funding from the Natural Sciences and Engineering Research Council of Canada, provision of the head model from the Global Human Body Models Consortium; and computational resources from the Digital Alliance of Canada. This research was undertaken, in part, thanks to funding from the Canada Research Chairs Program.

Bibliography

1. Albert, D. L. Variations in User Implementation of the CORA Rating Metric. , 2021.doi:10.4271/2020-22-0001
2. Alshareef, A., J. S. Giudice, J. Forman, R. S. Salzar, and M. B. Panzer. A Novel Method for Quantifying Human In Situ Whole Brain Deformation under Rotational Loading Using Sonomicrometry. *Journal of Neurotrauma* 35:780–789, 2018.
3. Alshareef, A., J. S. Giudice, J. Forman, D. F. Shedd, T. Wu, K. A. Reynier, and M. B. Panzer. Application of trilateration and Kalman filtering algorithms to track dynamic brain deformation using sonomicrometry. *Biomedical Signal Processing and Control* 56:101691, 2020.
4. Benko, N., E. Luke, Y. Alsanea, and B. Coats. Mechanical characterization of the human pia-arachnoid complex. *Journal of the Mechanical Behavior of Biomedical Materials* 120:104579, 2021.
5. Bustamante, M. C., and D. S. Cronin. Cavitation threshold evaluation of porcine cerebrospinal fluid using a Polymeric Split Hopkinson Pressure Bar-Confinement chamber apparatus. *Journal of the Mechanical Behavior of Biomedical Materials* 100:103400, 2019.
6. Cheng, S., and L. E. Bilston. Unconfined compression of white matter. *Journal of Biomechanics* 40:117–124, 2007.
7. Cronin, D. S. Explicit Finite Element Method Applied to Impact Biomechanics Problems. , 2011.
8. Deck, C., and R. Willinger. Improved head injury criteria based on head FE model. *International Journal of Crashworthiness* 13:667–678, 2008.
9. Dewan, M. C., A. Rattani, S. Gupta, R. E. Baticulon, Y.-C. Hung, M. Punchak, A. Agrawal, A. O. Adeleye, M. G. Shrime, A. M. Rubiano, J. V. Rosenfeld, and K. B. Park. Estimating the global incidence of traumatic brain injury. *Journal of Neurosurgery* 130:1080–1097, 2019.
10. Donnelly, B. R., and J. Medige. Shear Properties of Human Brain Tissue. *Journal of Biomechanical Engineering* 119:423–432, 1997.
11. Franceschini, G., D. Bigoni, P. Regitnig, and G. A. Holzapfel. Brain tissue deforms similarly to filled elastomers and follows consolidation theory. *Journal of the Mechanics and Physics of Solids* 54:2592–2620, 2006.
12. Fung, Y.-C. Bioviscoelastic Solids. In: Biomechanics: Mechanical Properties of Living Tissues, edited by Y.-C. Fung. New York, NY: Springer, 1993, pp. 242–320.doi:10.1007/978-1-4757-2257-4_7
13. Galbraith, J. A., L. E. Thibault, and D. R. Matteson. Mechanical and Electrical Responses of the Squid Giant Axon to Simple Elongation. *Journal of Biomechanical Engineering* 115:13–22, 1993.
14. Gayzik, F. S., D. P. Moreno, C. P. Geer, S. D. Wuertzer, R. S. Martin, and J. D. Stitzel. Development of a Full Body CAD Dataset for Computational Modeling: A Multi-modality Approach. *Ann Biomed Eng* 39:2568, 2011.
15. Gehre, C., and H. Gades. OBJECTIVE RATING OF SIGNALS USING TEST AND SIMULATION RESPONSES. , 2009.
16. Ghajari, M., P. J. Hellyer, and D. J. Sharp. Computational modelling of traumatic brain injury predicts the location of chronic traumatic encephalopathy pathology. *Brain* 140:333–343, 2017.
17. Giudice, J. S., A. Alshareef, T. Wu, A. K. Knutsen, L. V. Hiscox, C. L. Johnson, and M. B. Panzer. Calibration of a Heterogeneous Brain Model Using a Subject-Specific Inverse Finite Element Approach. *Frontiers in Bioengineering and Biotechnology* 9:, 2021.
18. Giudice, J. S., W. Zeng, T. Wu, A. Alshareef, D. F. Shedd, and M. B. Panzer. An Analytical Review of the Numerical Methods used for Finite Element Modeling of Traumatic Brain Injury. *Ann Biomed Eng* 47:1855–1872, 2019.
19. Gururaj, G. Epidemiology of traumatic brain injuries: Indian scenario. *Neurological Research* 24:24–28, 2002.
20. Hardy, W. N. Response of the Human Cadaver Head to Impact. , 2007.

21. Hardy, W. N., C. D. Foster, M. J. Mason, K. H. Yang, A. I. King, and S. Tashman. Investigation of Head Injury Mechanisms Using Neutral Density Technology and High-Speed Biplanar X-ray. , 2001.doi:10.4271/2001-22-0016
22. Hardy, W. N., M. J. Mason, C. D. Foster, C. S. Shah, J. M. Kopacz, K. H. Yang, A. I. King, J. Bishop, M. Bey, W. Anderst, and S. Tashman. A Study of the Response of the Human Cadaver Head to Impact. *Stapp Car Crash J* 51:17–80, 2007.
23. Hosseini-Farid, M., M. Ramzanpour, J. McLean, M. Ziejewski, and G. Karami. A poro-hyper-viscoelastic rate-dependent constitutive modeling for the analysis of brain tissues. *Journal of the Mechanical Behavior of Biomedical Materials* 102:103475, 2020.
24. Iwamoto, M., Y. Kisanuki, I. Watanabe, K. Furusu, K. Miki, and J. Hasegawa. Development of a Finite Element Model of the Total Human Model for Safety (THUMS) and Application to Injury Reconstruction
25. Ji, S., M. Ghajari, H. Mao, R. H. Kraft, M. Hajiaghamemar, M. B. Panzer, R. Willinger, M. D. Gilchrist, S. Kleiven, and J. D. Stitzel. Use of Brain Biomechanical Models for Monitoring Impact Exposure in Contact Sports. *Ann Biomed Eng* , 2022.doi:10.1007/s10439-022-02999-w
26. Jin, X., C. Ma, L. Zhang, K. H. Yang, A. I. King, G. Dong, and J. Zhang. Biomechanical Response of the Bovine Pia-Arachnoid Complex to Normal Traction Loading at Varying Strain Rates. , 2007.doi:10.4271/2007-22-0004
27. Jin, X., F. Zhu, H. Mao, M. Shen, and K. H. Yang. A comprehensive experimental study on material properties of human brain tissue. *Journal of Biomechanics* 46:2795–2801, 2013.
28. Khasawneh, A. H., R. J. Garling, and C. A. Harris. Cerebrospinal fluid circulation: What do we know and how do we know it? *Brain Circ* 4:14–18, 2018.
29. Kimpara, H., Y. Nakahira, M. Iwamoto, K. Miki, K. Ichihara, S. Kawano, and T. Taguchi. Investigation of Anteroposterior Head-Neck Responses during Severe Frontal Impacts Using a Brain-Spinal Cord Complex FE Model. , 2006.doi:10.4271/2006-22-0019
30. Kleiven, S., and W. N. Hardy. Correlation of an FE Model of the Human Head with Local Brain Motion-Consequences for Injury Prediction. , 2002.doi:10.4271/2002-22-0007
31. Li, Z., C. Ji, D. Li, R. Luo, G. Wang, and J. Jiang. A comprehensive study on the mechanical properties of different regions of 8-week-old pediatric porcine brain under tension, shear, and compression at various strain rates. *Journal of Biomechanics* 98:109380, 2020.
32. Li, Z., H. Yang, G. Wang, X. Han, and S. Zhang. Compressive properties and constitutive modeling of different regions of 8-week-old pediatric porcine brain under large strain and wide strain rates. *Journal of the Mechanical Behavior of Biomedical Materials* 89:122–131, 2019.
33. Lyu, D., R. Zhou, C. Lin, P. Prasad, and L. Zhang. Development and Validation of a New Anisotropic Visco-Hyperelastic Human Head Finite Element Model Capable of Predicting Multiple Brain Injuries. *Frontiers in Bioengineering and Biotechnology* 10:, 2022.
34. Mao, H. Chapter 12 - Modeling the Head for Impact Scenarios. In: Basic Finite Element Method as Applied to Injury Biomechanics, edited by K.-H. Yang. Academic Press, 2018, pp. 469–502.doi:10.1016/B978-0-12-809831-8.00012-X
35. Mao, H., L. Zhang, B. Jiang, V. V. Genthikatti, X. Jin, F. Zhu, R. Makwana, A. Gill, G. Jandir, A. Singh, and K. H. Yang. Development of a Finite Element Human Head Model Partially Validated With Thirty Five Experimental Cases. *Journal of Biomechanical Engineering* 135:, 2013.
36. Miller, L. E., J. E. Urban, and J. D. Stitzel. Development and validation of an atlas-based finite element brain model. *Biomech Model Mechanobiol* 15:1201–1214, 2016.
37. Nahum, A. M., R. Smith, and C. C. Ward. Intracranial Pressure Dynamics During Head Impact. , 1977.doi:10.4271/770922
38. Ogden, R. W. Large deformation isotropic elasticity – on the correlation of theory and experiment for incompressible rubberlike solids. *Proc. R. Soc. Lond. A* 326:565–584, 1972.

39. Pervin, F., and W. W. Chen. Dynamic mechanical response of bovine gray matter and white matter brain tissues under compression. *Journal of Biomechanics* 42:731–735, 2009.
40. Pervin, F., and W. W. Chen. Effect of inter-species, gender, and breeding on the mechanical behavior of brain tissue. *NeuroImage* 54:S98–S102, 2011.
41. Rashid, B., M. Destrade, and M. D. Gilchrist. Mechanical characterization of brain tissue in compression at dynamic strain rates. *Journal of the Mechanical Behavior of Biomedical Materials* 10:23–38, 2012.
42. Rycman, A., S. McLachlin, and D. S. Cronin. A Hyper-Viscoelastic Continuum-Level Finite Element Model of the Spinal Cord Assessed for Transverse Indentation and Impact Loading. *Frontiers in Bioengineering and Biotechnology* 9:, 2021.
43. Rycman, A., S. McLachlin, and D. S. Cronin. Comparison of numerical methods for cerebrospinal fluid representation and fluid–structure interaction during transverse impact of a finite element spinal cord model. *International Journal for Numerical Methods in Biomedical Engineering* 38:, 2022.
44. Rycman, A., S. D. McLachlin, and D. S. Cronin. Spinal Cord Boundary Conditions Affect Brain Tissue Strains in Impact Simulations. *Ann Biomed Eng* , 2022.doi:10.1007/s10439-022-03089-7
45. Sahoo, D., C. Deck, and R. Willinger. Development and validation of an advanced anisotropic visco-hyperelastic human brain FE model. *Journal of the Mechanical Behavior of Biomedical Materials* 33:24–42, 2014.
46. Schmitt, K.-U., P. F. Niederer, D. S. Cronin, B. Morrison III, M. H. Muser, and F. Walz. Head Injuries. In: Trauma Biomechanics: An Introduction to Injury Biomechanics, edited by K.-U. Schmitt, P. F. Niederer, D. S. Cronin, B. Morrison III, M. H. Muser, and F. Walz. Cham: Springer International Publishing, 2019, pp. 87–115.doi:10.1007/978-3-030-11659-0_4
47. Scott, G. G., S. S. Margulies, and B. Coats. Utilizing multiple scale models to improve predictions of extra-axial hemorrhage in the immature piglet. *Biomech Model Mechanobiol* 15:1101–1119, 2016.
48. Singh, D., S. Boakye-Yiadom, and D. S. Cronin. Comparison of porcine brain mechanical properties to potential tissue simulant materials in quasi-static and sinusoidal compression. *Journal of Biomechanics* 92:84–91, 2019.
49. Takhounts, E. G., R. H. Eppinger, J. Q. Campbell, R. E. Tannous, E. D. Power, and L. S. Shook. On the Development of the SIMon Finite Element Head Model. , 2003.doi:10.4271/2003-22-0007
50. Takhounts, E. G., S. A. Ridella, V. Hasija, R. E. Tannous, J. Q. Campbell, D. Malone, K. Danelson, J. Stitzel, S. Rowson, and S. Duma. Investigation of Traumatic Brain Injuries Using the Next Generation of Simulated Injury Monitor (SIMon) Finite Element Head Model. , 2008.doi:10.4271/2008-22-0001
51. Taylor, C. A., J. M. Bell, M. J. Breiding, and L. Xu. Traumatic Brain Injury–Related Emergency Department Visits, Hospitalizations, and Deaths — United States, 2007 and 2013. *MMWR Surveill. Summ.* 66:1–16, 2017.
52. Trotta, A., J. M. Clark, A. McGoldrick, M. D. Gilchrist, and A. N. Annaidh. Biofidelic finite element modelling of brain trauma: Importance of the scalp in simulating head impact. *International Journal of Mechanical Sciences* 173:105448, 2020.
53. Zhang, L., K. H. Yang, R. Dwarampudi, K. Omori, T. Li, K. Chang, W. N. Hardy, T. B. Khalil, and A. I. King. Recent Advances in Brain Injury Research: A New Human Head Model Development and Validation. , 2001.doi:10.4271/2001-22-0017
54. Zhao, W., and S. Ji. Mesh Convergence Behavior and the Effect of Element Integration of a Human Head Injury Model. *Ann Biomed Eng* 47:475–486, 2019.
55. Zhao, W., and S. Ji. Displacement- and Strain-Based Discrimination of Head Injury Models across a Wide Range of Blunt Conditions. *Ann Biomed Eng* 48:1661–1677, 2020.
56. Zhou, Z., X. Li, S. Kleiven, C. S. Shah, and W. N. Hardy. A Reanalysis of Experimental Brain Strain Data: Implication for Finite Element Head Model Validation. , 2018.doi:10.4271/2018-22-0007